CHAPTER-5

A Peroxidase-Mimicking Single Nucleobase Bionanozyme for Biomedical Applications

5.1 Introduction:

Peroxidase (POD) is the second-largest enzyme in the oxidoreductases class used in biotechnological processes.[1] POD's are ubiquitous enzymes found in both eukaryotic and prokaryotic organisms, where they protect the cells against the effects of oxidative stress and cell damage caused by endogenous hydrogen peroxide (H_2O_2). PODs also efficiently catalyze the reduction of peroxides at the expense of many kinds of electron-donating substrates. These unique biocatalytic abilities make POD enzymes significant interest in diverse biotechnological and industrial applications including biosensors, medicine, food industry, agrochemicals, and environmental protection.[2,3] PODs are also extensively employed in clinical chemistry and bioanalytical applications for the colorimetric assay-based analyte detection. On the downside, POD enzymes are often expensive in preparation and purification, sensitive to harsh physiochemical conditions, low operation stability, unstable to transfer or modify, difficulties in recover and recycling, which greatly hinders their practical applications.[4] To address the aforementioned limitations, the *de novo* design of low-cost, effective, and highly stable artificial enzymes mimics called nanozymes have been reported.[5] Consequently, nanozymes are the nanomaterials with enzyme-like biocatalytic properties intriguing researchers as new artificial enzymes.[6] Due to their intrinsic advantages of high stability, low cost, and adaptable catalytic activity, nanozymes demonstrated significant potential for the interchangeable usage of their natural counterparts. Towards this goal of developing nanozymes numerous attempts have been made to design and synthesize various nanomaterials including metal oxides, metal sulphides, noble metals, metal-organic frameworks (MOFs) and carbon-based nanomaterials. The most of these nanozyme studies concentrate on mimicking oxidoreductases (POD, catalase (CAT), oxidase (OXD), and superoxide dismutase (SOD)) biocatalytic activity, and few extending to hydrolases activity such as phosphatase and urease.[7] The first POD mimicking nanozyme was described in 2007 utilizing Fe_3O_4 nanoparticles.[8] Later, it was discovered that some Fe(II) -based nanocomposites had POD-like activity by converting H_2O_2 to O_2 and hydroxyl radicals through the Fenton oxidation mechanism.[9] In an effort to overcome the limitations of Fe(II) stability and narrow pH range activity, copper ions have recently been employed in place of iron ions to produce POD-mimicking nanozymes that act through a process known as the Fenton-like reaction.[10–12] About more than 40 nanozymes have been discovered so far that display POD-like activity.[13] However, the majority of the reported nanozymes are made up of inorganic-based nanomaterials that bear no resemblance to the native enzyme's structure and properties. This restricts the rational path toward the mechanistic understating of enzymes and the minimalistic design of artificial enzymes. Additionally, their

biomedical applications are constrained by harsh and time-consuming synthetic conditions, intricate fabrication processes, expensive machinery, toxic nature, and low specificity.[14] Moving on to more minimalistic approach we have developed a Peroxidase (POD) mimicking bionanozyme by employing coordination chemistry approach between nucleobase Adenine (A) and Cu^{2+}. When A coordinated with Cu^{2+} it forms stable, 2D crystals, and the resultant material called as 'A-Cu'. It is interesting to note that, the primary coordination sphere of A-Cu bionanozyme contains histidine like Nitrogen (N) coordination (from the adenine molecules) with co-facto (Cu^{2+}) which is resembles to the active site of peroxidase (POD) enzyme which is composed of histidine N-atoms coordinated with metal co-factor. After taking inspiration from this structural resemblance between the active site of A-Cu and the active site of POD-enzymes, we tried to mimic the POD-like activity by using the A-Cu bionanozyme. In this chapter we are going to demonstrates the excellent POD like biocatalytic performance of A-Cu bionanozyme. We have employed the Fenton-like reaction pathway, to displayed efficient catalytic conversion of H_2O_2 into H_2O through the generation of Reactive oxygen species (ROS) under mild physiological conditions in presence of A-Cu bionanozyme. Furthermore, this catalytic conversion was successfully applied to the development of ultrasensitive colorimetric methods for the detection of Biomarker H_2O_2 and neurotransmitters GSH, furthermore biocompatibility, and *in-vivo* ROS scavenging was successfully studied.

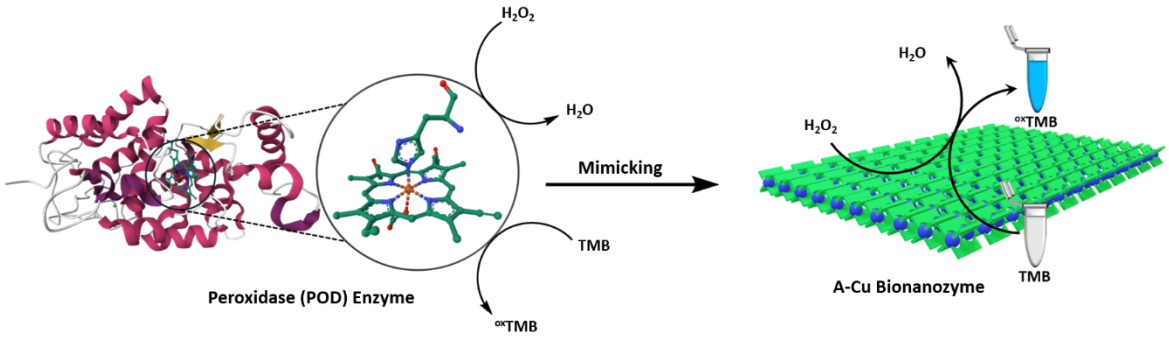

Figure 1. POD-Mimicking activity of A-Cu bionanozyme, by catalysing the conversion of H_2O_2 into H_2O. Colorimetric substrate TMB used to monitor this conversion visually and spectroscopically.

5.2 Results and Discussion:

5.2.1 Synthesis and Characterization of Single Nucleobase-derived Bionanozyme:

(Note: Please refer to chapter-4, for the detailed synthesis procedure and characterization of A-Cu bionanozyme)

5.2.2 POD-mimicking assay of A-Cu Bionanozyme for the detection of H_2O_2 and GSH:

The POD-mimicking biocatalytic activity of the A-Cu Bionanozyme was evaluated using hydrogen peroxide (H_2O_2) and the benchmark POD substrate 3,3′,5,5′-tetramethylbenzidine (TMB). As shown in **Figure 2a**, the catalytic decomposition of H_2O_2 by the A-Cu Bionanozyme converts to H_2O; during this reaction, colorless TMB molecules are oxidized to a deep blue chromogenic product (^{ox}TMB), which shows a characteristic absorbance at 652 nm **(Figure 2d**).[15] Upon the addition of A-Cu to a colorless mixture of H_2O_2 and TMB in PBS buffer of optimum pH (1X, pH 4, at 24°C), an immediate color change to deep blue was observed, along with a broad absorbance band in the visible region with λ_{max} at 652 nm **(Figure 2b).** This confirms the intrinsic POD-mimicking biocatalytic capability of the A-Cu Bionanozyme. In contrast, control solutions containing H_2O_2, TMB, A-Cu alone, and combinations of H_2O_2+TMB, H_2O_2+A-Cu, and TMB+A-Cu did not show any significant visible color change or absorbance band, indicating the absence of background reactions **(Figure 2c)**. The pH-dependent studies revealed that the acidic pH 4 is optimal for A-Cu POD-mimicking activity **(Figure 3a).** Next, the POD-activity of A-Cu was tested in acetate buffer also, it is interesting to note that more reaction progress was observed in the case of PBS buffer at optimum pH **(Figure 3b)**.

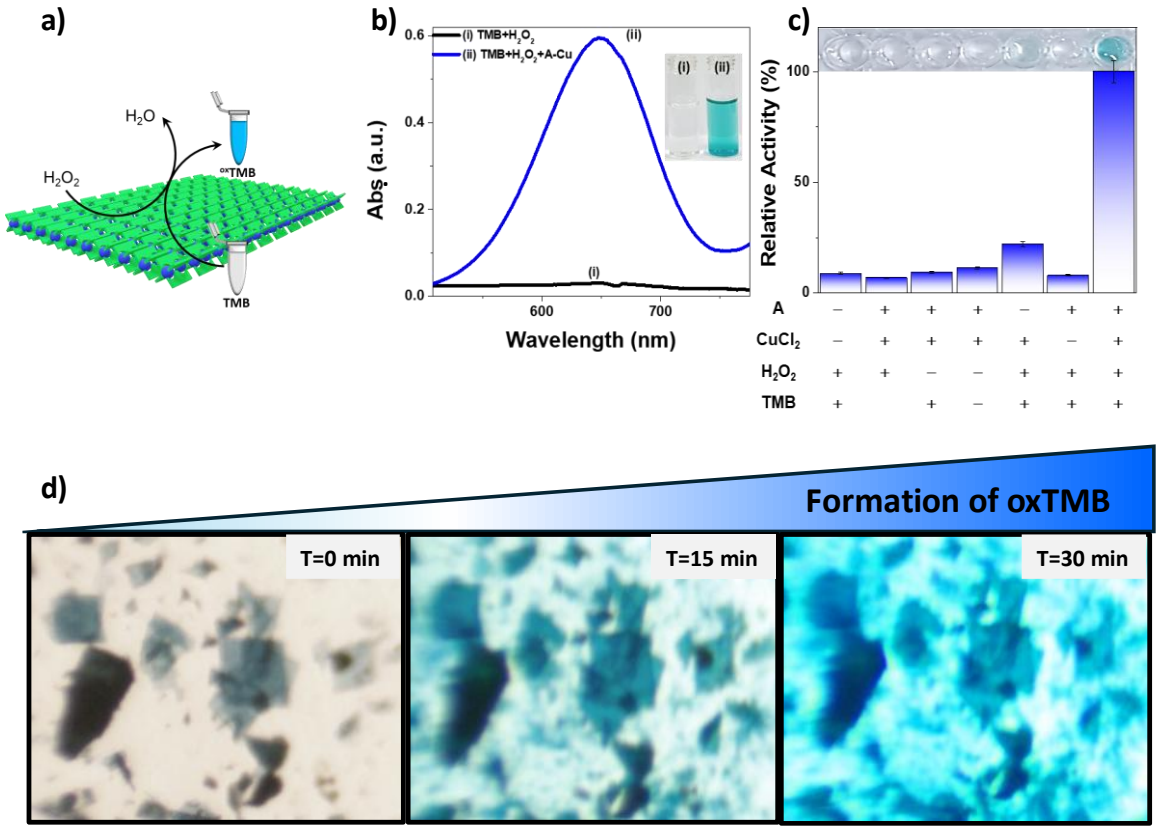

Figure 2. (a) Schematic illustration of the POD-mimicking catalytic characteristics of the A-Cu Bionanozyme for colorimetric detection of H_2O_2 and GSH. **(b)** UV-vis absorption spectra of the substrates (H_2O_2 + TMB) alone and in the presence of the A-Cu Bionanozyme. Inset: corresponding photographs of the reaction vials. **(c)** The relative catalytic activity is demonstrated through various control experiments. Inset: corresponding photographs of the reaction wells. **(d)** Optical microscopy snapshots at different intervals (0 min, 15 min, and 30 min) taken from the in-situ reaction monitoring of TMB catalyzed by A-Cu crystals, displaying the solution color change going from colorless (at 0 min) to red (after 30 min).

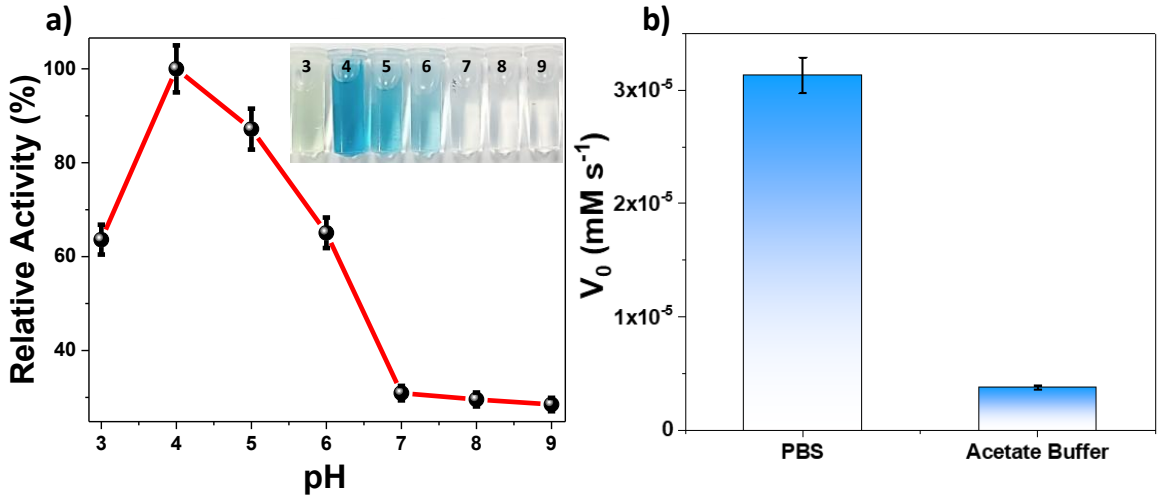

Figure 3. (a) pH-dependent relative POD-mimicking catalytic activity of the A-Cu Bionanozyme. Inset: corresponding photographs of the reaction vials. **(b)** Comparison of the POD-like activity of A-Cu in acetate buffer and PBS buffer, notably A-Cu displayed more activity in PBS buffer as compared to acetate buffer.

Next, to elucidate the reaction kinetics, reaction rates were measured under optimum constant catalyst (A-Cu) concentration (0.2 mg/mL, **Figure 4a)** and constant optimum concentration of TMB (0.2 mM, **Figure 4b**) with varying concentrations of substrate H_2O_2. The enzyme-like kinetics of the A-Cu Bionanozyme are evident from the relationship between the initial reaction rate and substrate H_2O_2 concentration **(Figure 4c**). An exponential increase in reaction rate was observed, which subsequently plateaued, indicating that further increases in substrate (H_2O_2) concentration did not significantly impact the reaction rate. The initial reaction velocity concerning substrate concentration fits well with the MM equation **(Figure 4d)**. From the MM fitting analysis, the maximum reaction rate (V_{max}) and the MM constant (K_m) were extracted and compared with literature values **(Table 1)**. For the substrate H_2O_2, A-Cu exhibited kinetic parameters with a V_{max} of 8.14×10^{-5} mM/sec, K_m of 0.0848 mM, and a calculated k_{cat} value of 9.276/sec.[8] Notably, the lower K_m and higher V_{max} values for A-Cu Bionanozymes indicate a higher substrate binding affinity and almost equal rate of catalysis as compared to natural HRP enzymes.

Table 1. Comparison of the kinetics parameters for the peroxidase-like activity of different biomolecular nanozymes.

Material	**Substrate**	**K_m (mM)**	**V_{max}(mM/sec) $\times10^{-5}$**	**K_{cat} (sec^{-1})**	**Ref.**
A-Cu	**H_2O_2**	**0.0848**	**8.145**	**9.276**	**This Work**
Mn_3O_4 NPs	TMB	0.025	5.1	5×10^{-4}	[16]
Naked-Fe_3O_4	H_2O_2	111	15.2	3.93×10^{-5}	[17]
Ala-Fe_3O_4	H_2O_2	226.6	0.445	4.54×10^{5}	[18]
His-Fe_3O_4	H_2O_2	37.99	0.528	5.39×10^{5}	
HRP	H_2O_2	5.2	0.803	3.21×10^{4}	[19]

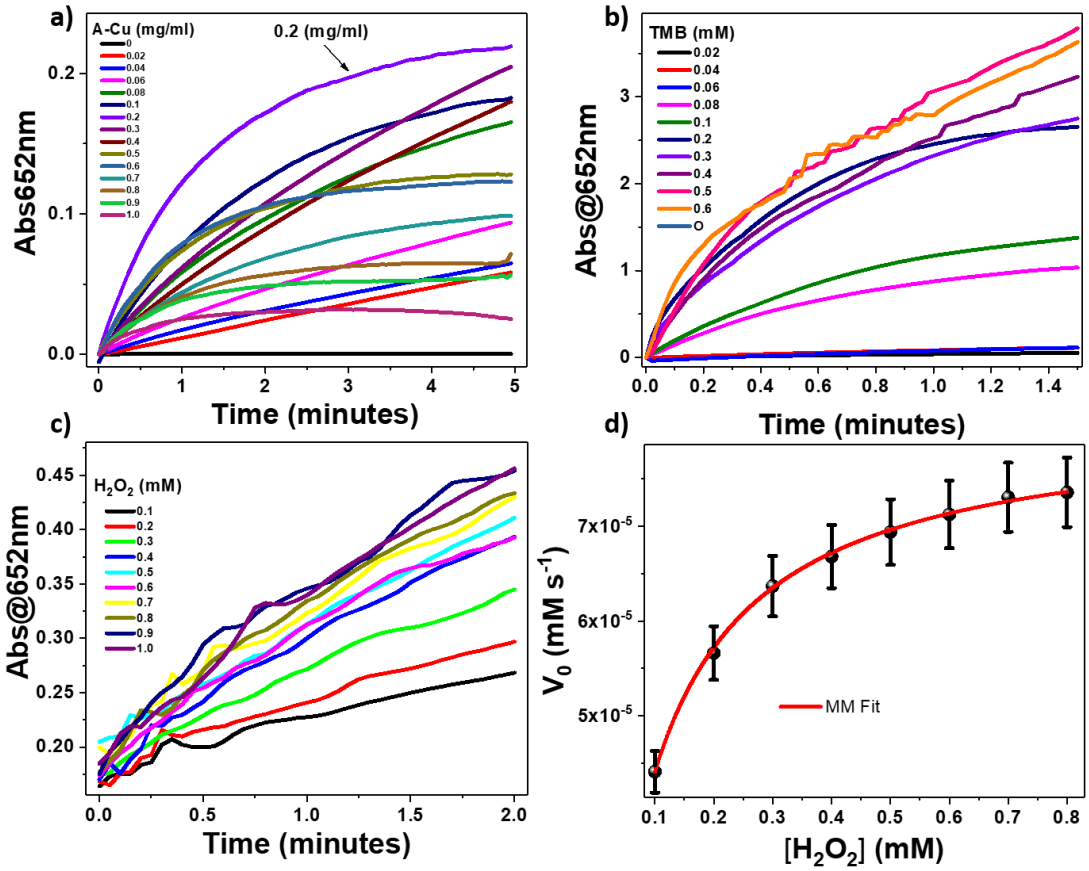

Figure 4. (a) Kinetics studies for the optimization of A-Cu amount in mg/ml with fixed TMB (0.2 mM) and H_2O_2 (1 mM) concentration at pH-4 at room temperature, 0.2 mg/ml amount of A-Cu shows the best enzyme-like increment pattern with maximum slope value. **(b)** Kinetics for the optimization of the concentration of substrate TMB, results show the best enzyme-like increment pattern at 0.2 mM concentration of TMB with fixed A-Cu and H_2O_2 concentrations. (**c)** Substrate-dependent kinetics with varying range of H_2O_2 concentration (0.1, 0.2, 0.3, 0.4, 0.5, 0.6, 0.7, 0.8, 0.9, 1.0 mM) with fixed and optimum concentration of A-Cu and TMB. **d)** The initial reaction rate (V_0) catalyzed by the A-Cu Bionanozyme (0.2 mg/mL) is plotted against the concentration of H_2O_2 ([TMB] = 0.2 mM), and the data are fitted using the Michaelis-Menten model.

Moreover, to gain insight into the catalytic mechanism through which A-Cu decomposes H_2O_2, the involvement of reactive oxygen species (ROS) was investigated **(Figure 5a)**. Superoxide radicals ($O_2^{\bullet-}$) were selectively scavenged using p-benzoquinone (PBQ), while hydroxyl radicals ($OH^{\bullet}$) were scavenged with isopropanol (IPA).[20–22] Experiments involving the co-incubation of A-Cu, H_2O_2, and TMB with either PBQ, IPA, or both combinations revealed a significant decrease in relative activity. Notably, IPA led to approximately a 50% reduction in activity, whereas PBQ resulted in about a 10% decrease. This suggests that both $OH^{\bullet}$ and $O_2^{\bullet-}$ play a crucial role in the oxidation of TMB. Additionally, EPR spectroscopy confirmed the presence of $OH^{\bullet}$ radicals specifically in the reaction mixture of A-Cu+H_2O_2 +DMPO **(5,5-**

dimethyl-1-pyrroline N-oxide).[23] This was evident from a characteristic 1:2:2:1 quartet signal, indicative of a relatively stable paramagnetic adduct **(Figure 5b)**. In comparison, control reactions involving H_2O_2+DMPO and DMPO did not produce significant EPR signals, further reinforcing the notion that $OH^{\bullet}$ radicals are generated during the catalytic decomposition of H_2O_2 by the A-Cu Bionanozyme. Hence, both the UV-vis radical scavenging experiments and EPR spectroscopy strongly suggest that both $OH^{\bullet}$ and $O_2^{\bullet-}$ contribute to TMB oxidation, thus supporting a Fenton-like catalytic mechanism for the POD-mimicking A-Cu Bionanozyme **(Figure 5c, d)**.[24]

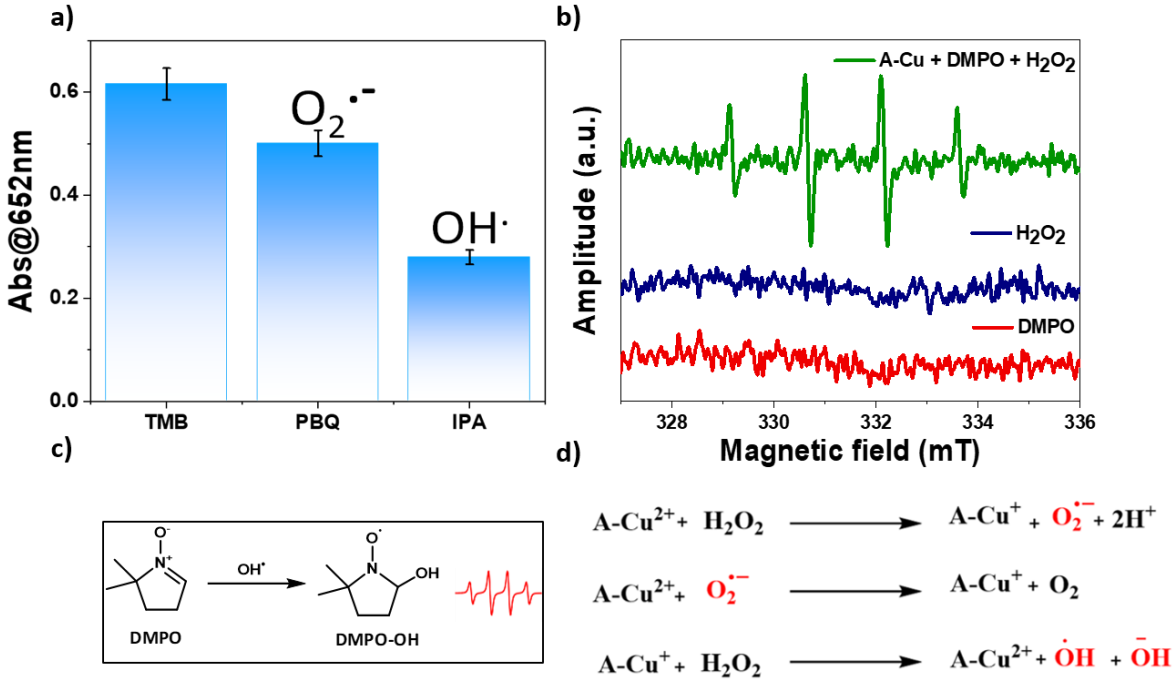

Figure 5. (a) ROS scavenging experiment clearly shows the diminishing band of ^{ox}TMB product with Parabenzoquinone (superoxide radical scavenger) and isopropanol (hydroxyl radical scavenger)**. (b)** Electron Paramagnetic Resonance (EPR) spectra of selected reaction mixtures, including DMPO, DMPO+H_2O_2 and A-Cu+DMPO+H_2O_2 in phosphate-buffered saline (PBS) at pH 4. **(c)** Schematic reaction showing the reaction between DMPO with OH radicals and the resultant product is EPR active in nature. **(d)** The proposed Fenton-like POD-mimicking catalytic mechanism of A-Cu Bionanozyme and oxidation of TMB.

Furthermore, the absorbance of ^{ox}TMB at 652 nm is directly proportional to the concentration of H_2O_2, enabling the quantitative assessment of H_2O_2 based on the catalytic activity of the A-Cu Bionanozyme. The absorbance intensity at 652 nm increased progressively with the H_2O_2 concentration, ranging from 10 to 140 µM **(Figure 6a)**. This change was also visually apparent, transitioning from colorless to blue, as shown in **Figure 6b** inset, providing an immediate

visual indication. A linear relationship was observed within the concentration range of 10 to 90 µM, allowing the calculation of the limit of detection (LOD) for H_2O_2 to be 6.8 µM **(Figure 6b)**. Notably, this LOD is comparable to or superior to those reported for the nanozyme-based detection of H_2O_2 **(Table 2)**. A visual change from colorless to blue was observed concurrently with the increase in absorbance. This qualitative observation further supports the potential of the A-Cu Bionanozyme as a colorimetric probe for H_2O_2 detection. The results collectively underscore the efficacy of the A-Cu Bionanozyme in catalyzing the oxidation of TMB by H_2O_2, providing a reliable and sensitive platform for colorimetric H_2O_2 quantification.

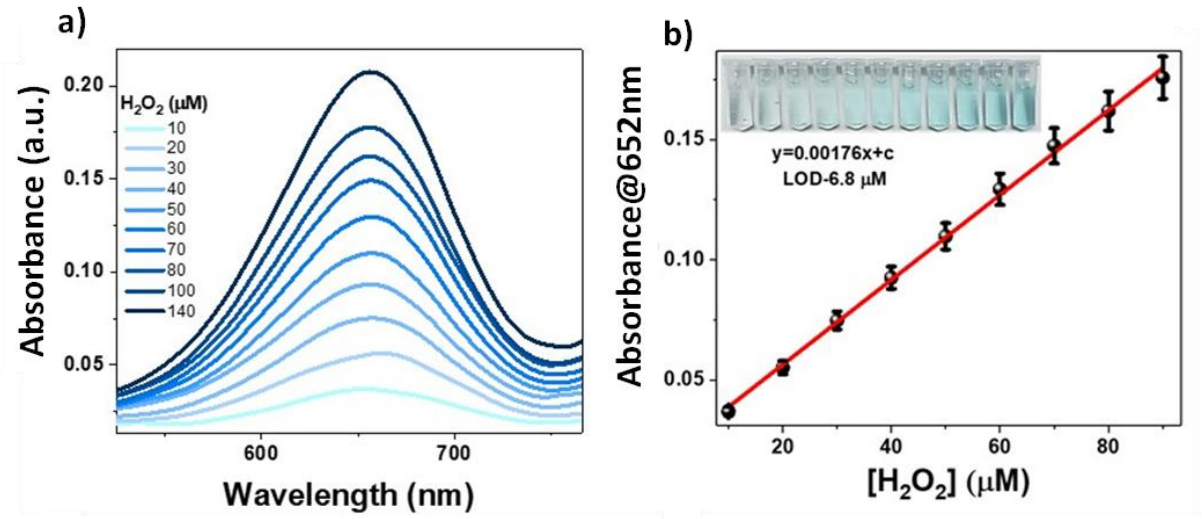

Figure 6. (a) This figure shows the increase in the absorbance band at 652 nm (for ^{ox}TMB) with an increase in the concentration of H_2O_2 with fixed A-Cu (0.2 mg/ml) and TMB (0.2 mM) in the concentration range of 10 to 140 µM. **(b)** A standard linear curve showing absorbance at 652 nm in relation to H_2O_2 concentration, with corresponding photographs in the inset.

Table 2. Comparison of LOD for the detection of H_2O_2 by using different methods and materials.

Nanomaterial	Method	LOD (μM)	Linear range (μM)	Ref.
FePt-Au HNPs	Colorimetric	12.33	20–700	[25]
Fe-Ag_2S	Colorimetric	7.82	10–150	[26]
CoS	Colorimetric	20	50–800	[27]
$Cu_2(OH)_3Cl$-CeO_2 nanocomposite	Colorimetric	10	20~50	[28]
Fe_3O_4@AuNPs	Colorimetric	11.1	40–5500	[29]
VB6	Colorimetric	12.1	50–600	[30]
Au−Ag−Pt Nanoparticle	Colorimetric	54	0-1000	[31]
A-Cu	**Colorimetric**	**6.8**	**10-90**	**This work**

5.2.3 Detection of antioxidant compound Glutathione (GSH):

GSH, a ubiquitous thiol-containing molecule in human tissues, is critical in maintaining intracellular redox homeostasis through the interconversion of Glutathione (GSH) to its oxidized Glutathione disulfide (GSSG).[32] Fluctuations in GSH levels are implicated in various pathologies, including cardiovascular diseases, diabetes, cancer, and neurodegenerative disorders.[33,34] Therefore, establishing rapid and accurate methods for GSH detection is crucial. Conventional GSH detection techniques often rely on reactions with its thiol group. Inspired by the robust POD-mimicking activity of A-Cu Bionanozyme, a sensing system for GSH detection was constructed using A-Cu mediated by TMB and H_2O_2. The proposed sensing system leverages the POD-like activity of A-Cu to oxidize TMB to its blue oxidized form (^{ox}TMB) in the presence of H_2O_2. Subsequently, GSH reduces ^{ox}TMB to colourless TMB, generating a signal amplification effect through color change **(Figure 7a)**. As depicted in **Figure 7b**, the detection sensitivity exhibits a concentration-dependent trend with GSH. A standard curve **(Inset Figure 7b)** constructed from the change in absorbance at 652 nm versus GSH concentration demonstrated a linear relationship within the 0-80 μM range. Moreover, upon evaluating the A-Cu+TMB+H_2O_2 system, the calculated LOD was 2 μM **(Table 3)**.

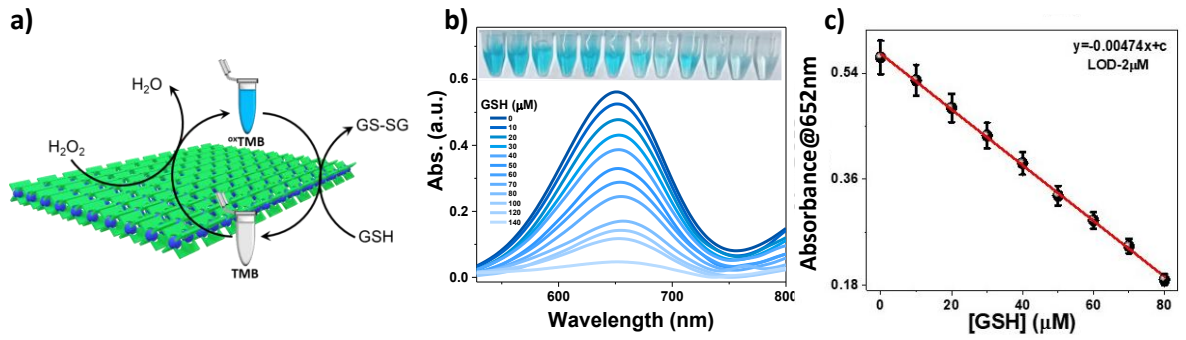

Figure 7. (a) Schematics showing the reduction of ^{ox}TMB molecules into reduced colourless TMB molecules on the addition of GSH molecules. **(b)** UV-vis absorption spectra of the incremental addition of GSH to the A-Cu + H_2O_2 + TMB reaction mixture along with corresponding photographs of the reaction vials. **(c)** Standard linear curve showing absorbance at 652 nm against GSH concentration,

Table 3. Comparison of LOD for the detection of GSH by using different methods and materials.

Nanomaterial	Method	LOD (μM)	Linear Range (μM)	Ref.
$Cu_{1.8}S$ nanoparticles	Colorimetric	6	500–10000	[35]
NixFe-MOF	Colorimetric	1.8	10-400	[36]
$H_2TCPP/Co(OH)_2/GO$	Colorimetric	9.5	10-300	[37]
Fe_3O_4 MNPs	Colorimetric	3	3-30	[38]
Au NPs–Hg(II)	Colorimetric	17	0.025–2.28	[39]
A-Cu	**Colorimetric**	**2**	**0-80**	**This Work**

This A-Cu-based sensing system offers superior sensitivity to existing colorimetric approaches. To evaluate selectivity, the system was challenged with various common biomolecules potentially present in biological samples, including Arginine, Lysine, Aspartic acid, Threonine, Tryptophan, Valine, Alanine, Isoleucine, Serine, Methionine, Glutathione (GSH), Histidine, Phenylalanine, Tyrosine, Proline, Asparagine, Glutamine, Glutamic Acid, cysteine and Cystine. As shown in **Figure 8**, these interferences caused negligible (ΔA/A) signal changes compared to GSH, indicating excellent selectivity of A-Cu Bionanozyme towards GSH. In addition, the inset picture in **Figure 8** also correlates with a change in the value of ΔA/A with color change in the case of analyte GSH (C1). GSH exhibits selective detection over cysteine, despite both being thiol (-SH)-containing compounds, due to its more complex structural characteristics. GSH possesses additional ionizable functional groups, including two carboxylic acid groups and one thiol group, which enhance its reactivity.[40–42] These features

enable GSH to interact with oxidized ^{ox}TMB more effectively than cysteine, resulting in a stronger reducing capability. More number of ionizable groups in GSH facilitates a more efficient reduction of ^{ox}TMB compared to cysteine, contributing to its higher selectivity in detection. Hence, this work highlights the potential of A-Cu Bionanozymes for developing sensitive and selective GSH detection systems, paving the way for improved monitoring of redox status in disease contexts.

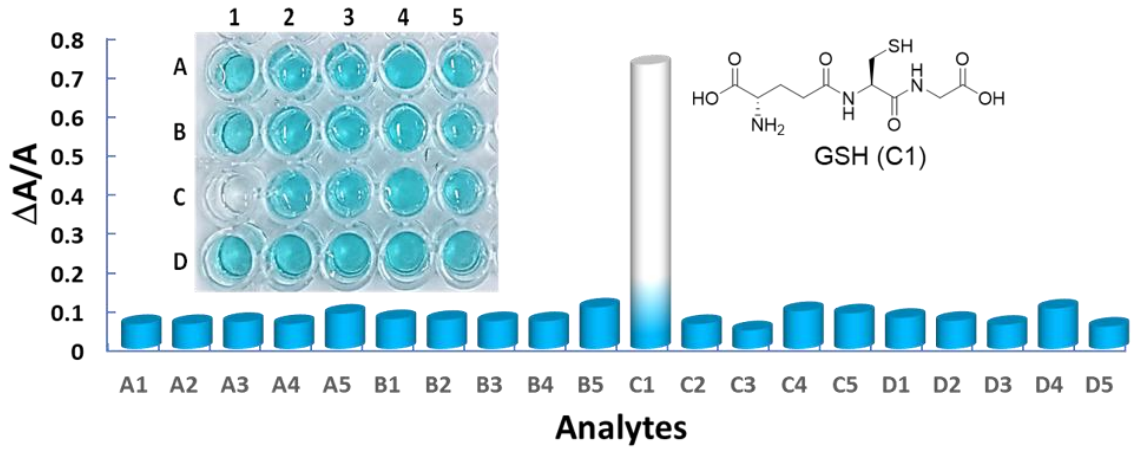

Figure 8. Interference experiment: ΔA/A ((A_0 - A) / A) versus various analytes. From left to right: A1 = L-Arginine, A2 = L-Lysine, A3 = L-Aspartic Acid, A4 = L-Threonine, A5 = L-Tryptophan, B1 = L-Valine, B2 = L-Alanine, B3 = L-Isoleucine, B4 = L-Serine, B5 = L-Methionine, C1 = L-Glutathione (GSH), C2 = L-Histidine, C3 = L-Phenylalanine, C4 = L-Tyrosine, C5 = L-Proline, D1 = L-Asparagine, D2 = L-Glutamine, D3 = L-Glutamic Acid, D4 = L-Cysteine, D5 = L-Cystine. Inset: corresponding photograph of the reaction well plate.

5.3 Biocompatibility and ROS scavenging property of A-Cu Bionanozyme:

5.3.1 A-Cu are non-toxic to embryonic fibroblast cell lines evaluated by MTT assay in a dose-dependent manner:

The preliminary nano-catalytic therapeutic efficiency of A-Cu Bionanozyme was evaluated *in vitro* through cellular cytotoxicity assays utilizing the well-established MTT (3-(4,5-dimethylthiazol-2-yl)-2,5-diphenyl tetrazolium bromide) method. The MTT assay was employed to assess the impact of A-Cu on the proliferation of the NIH3T3 embryonic fibroblast mouse cell line's **(Figure 9a)** capacity to sustain cell growth.[43] The results indicated that A-Cu did not exhibit significant cytotoxicity across a dose range of 0.1 mg/mL to 0.5 mg/mL. However, at a higher concentration of 1 mg/mL, A-Cu inhibited cell proliferation, demonstrating cytotoxic effects as illustrated in Figure 6a. These findings suggest that A-Cu is biocompatible and can be safely utilized for various biological applications at treatment doses up to 0.5 mg/mL.

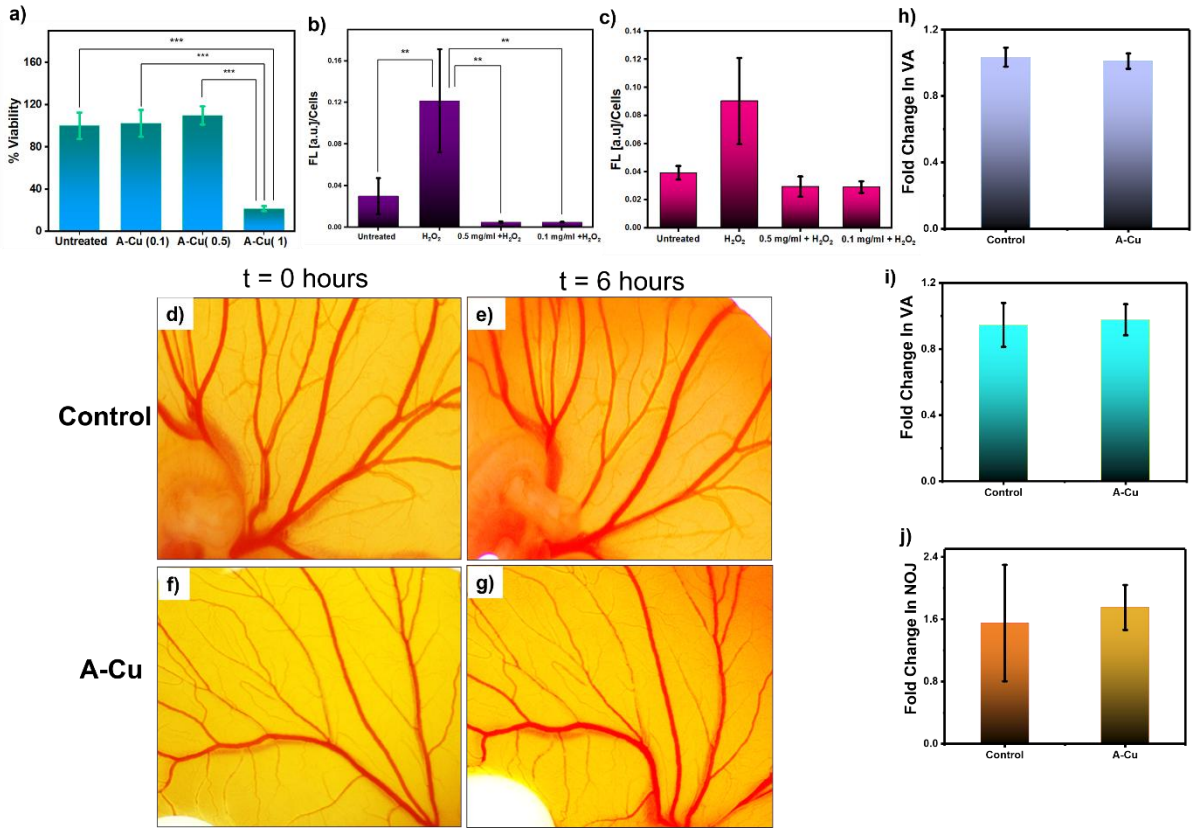

Figure 9. (a) MTT assay of A-Cu treated NIH3T3 cell lines showing cytocompatibility with varying doses. **b, c)** The elevated fluorescence intensity is shown by (**b)** KBCHR8 cells, and (**c)** HEK-293T with H_2O_2. In contrast, A-Cu at concentrations 0.1 mg/mL and 0.5 mg/mL showed a significant decrease in the fluorescence intensity with respect to untreated cells and cells treated with hydrogen peroxide, therefore showing efficiency in scavenging reactive oxygen species (ROS) and reducing oxidative damage. **(d-g)** The microscopic pictures of the untreated and A-Cu treated chick embryo models at 0 and 6 hours are displayed in a–d. **(h-j)** These figures are quantified in terms of area, length, and junction using tools such as ImageJ and Angiotool (VA denotes 'Vessel Area' and NOJ denotes 'Number of Junctions'). The three test results are displayed as mean±SD. There are no appreciable differences from embryos that were not treated (*p>0.05).

5.3.2 Application of A-Cu for the scavenging reactive oxygen species in live cells:

The H_2O_2 scavenging activity of A-Cu in test tube conditions encouraged us to extend further studies in cell lines. Reactive oxygen species (ROS) scavenging using nanomaterials has been explored extensively using various cancer (KBCHR8) and normal (HEK-293T) cell lines. ROS reduction is the ability to reduce the reactive oxygen species (ROS), which significantly causes cell death due to oxidative stress.[44] Nanomaterials with ROS-inhibiting ability are biocompatible and can be employed further for other biological applications. The most common ROS is hydrogen peroxide (H_2O_2) in all aerobic species. To confirm the ROS scavenging properties of A-Cu on the removal of H_2O_2 in biological settings, *in vitro* studies were performed using cancer (KBCHR8) and normal (HEK-293T) cell lines treated with H_2O_2 followed by A-Cu at varying concentrations **(Figure 9b, and c).** Each sample's fluorescence

intensity was assessed following DCFDA staining, demonstrating that A-Cu displayed antioxidant activity by successfully scavenging the cellular H_2O_2 **(Figure 10)**. Hence, treatment of A-Cu can mitigate oxidative damage by the H_2O_2 scavenging activity in cell lines. The Fluorescence images representing the H_2O_2 scavenging activity of A-Cu are represented **(Figure 11a)**

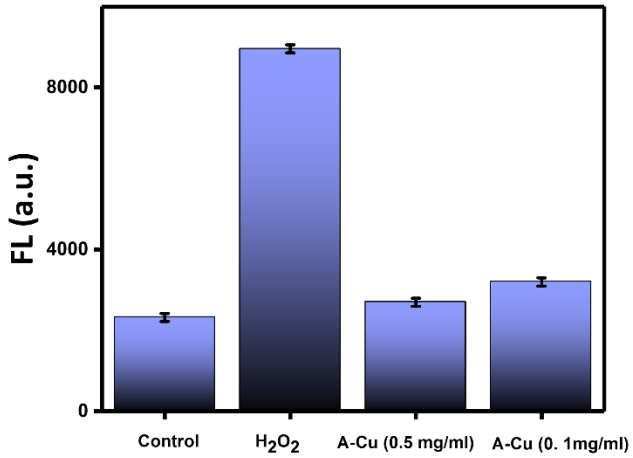

Figure 10. Fluorescence intensity measurement of DCFDA confocal.

5.3.3 A-Cu proved to be *in vivo* biocompatible in a study using chicken eggs:

The Chorioallantoic Membrane Assay (CAM) measures alterations in blood vessel development and junctions to determine whether a material is compatible with the live tissue of fertilized chicken eggs.[45] Using a stereo microscope, blood vessel pictures of chick embryos were taken at various intervals up to six hours after treatments were applied **(Figure 9d-g)**. This experiment shows that A-Cu treatments did not disrupt vascular architecture or blood vessel formation in chick embryos. Numerous blood vessel integrity-related metrics, including size, length, and junctions, were quantified to show that all the parameters are constant throughout all the samples without any significant changes **(Figure 9h-j)**. Overall, the findings are consistent with the A-Cu's biocompatibility, which is crucial for its safe biomedical applications.

5.3.4 Live Dead Assay:

The cytoprotective effect of the A-Cu complex under oxidative stress was validated using a live/dead cell imaging kit, which employs Component A, calcein-AM (indicating viable cells with green fluorescence), and Component B (indicating dead cells with red fluorescence). As shown in **Figure 11b**, cells treated solely with H_2O_2 exhibited primarily red fluorescence and minimal green fluorescence, indicating significant membrane damage and a decrease in cell

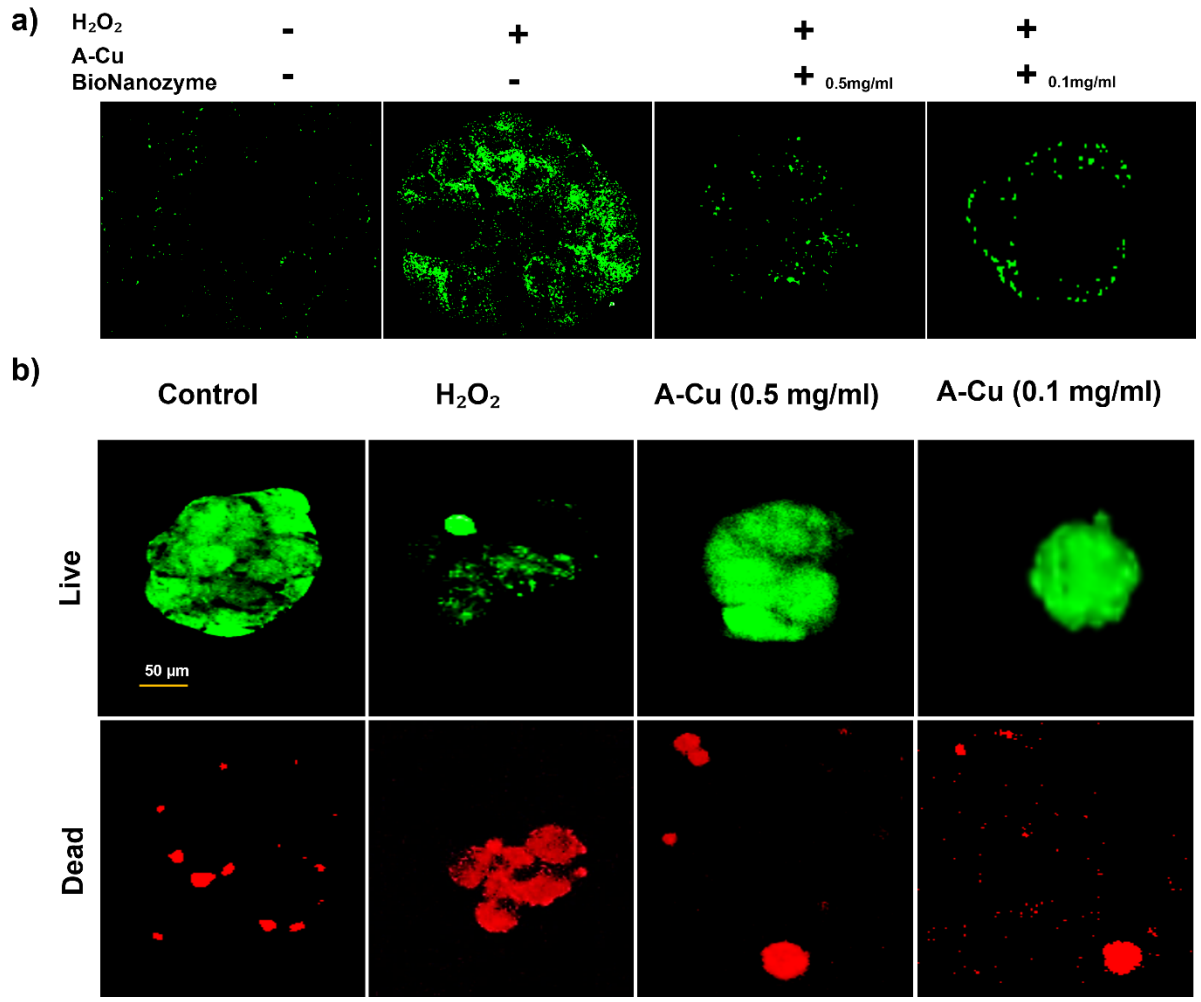

Figure 11. Fluorescence imaging of A-Cu scavenging reactive oxygen species in live cells and results from the Live/Dead assay. **a)** Treatment of HEK-293T cells with H_2O_2 resulted in elevated fluorescence, indicating increased levels of reactive oxygen species (ROS). Conversely, A-Cu at concentrations of 0.5 mg/mL and 0.1 mg/mL significantly reduced fluorescence compared to untreated cells and those treated with H_2O_2, demonstrating its efficacy in scavenging ROS and mitigating oxidative damage. **b)** The Live/Dead assay illustrated that HEK-293T cells exposed to H_2O_2 had a reduced number of live cells (indicated in green) and an increased number of dead cells (indicated in red). In contrast, the presence of A-Cu at concentrations of 0.1 mg/mL and 0.5 mg/mL in conjunction with H_2O_2 led to a notable increase in cell viability, further highlighting its role in reducing oxidative stress.

viability due to oxidative injury. This finding aligns with the activation of apoptotic and necrotic pathways caused by elevated levels of reactive oxygen species (ROS).[46] In contrast, cells co-treated with A-Cu at concentrations of 0.1 mg/mL and 0.5 mg/mL in the presence of H_2O_2 demonstrated a notable increase in green fluorescence and a substantial reduction in red fluorescence. These results imply that A-Cu effectively protects cells by mitigating oxidative membrane damage and enhancing cell survival. Notably, the 0.5 mg/mL dose group showed near-complete restoration of cell viability, comparable to that of untreated control cells, thereby underscoring its protective capability. Interestingly, the positive control group—which

consisted of cells not exposed to either H_2O_2 or A-Cu—exhibited uniformly green fluorescence, suggesting a population of healthy and viable cells. The similarity in fluorescence intensity between the positive control and the A-Cu-treated groups indicates the potential of A-Cu as an effective Bionanozyme for restoring cellular homeostasis in the context of oxidative stress.
Overall, these findings highlight the dual role of the A-Cu complex as both a ROS scavenger and a cytoprotective agent. Its ability to lower ROS levels and maintain cell viability under oxidative stress positions as a promising candidate for biomedical applications aimed at addressing oxidative damage, including neurodegeneration, ischemia-reperfusion injury, and inflammatory disorders. The nanoscale integration of adenine scaffolds with copper ions likely creates a synergistic effect that combines intrinsic antioxidant properties with enzymatic mimicry.[47] Additionally, the non-toxic nature of A-Cu in control experiments suggests favorable biocompatibility, a crucial factor for its potential therapeutic applications.

5.4 Conclusion

In summary, this chapter presents the rational design and successful synthesis of a novel single Nucleobase-based bionanozyme, referred to as A-Cu. The engineered bionanozyme not only exhibited excellent laccase (LAC) and catechol oxidase (COs)-mimicking activities (Chapter 4) but was also strategically employed for its peroxidase (POD)-like catalytic behaviour. This was inspired by the striking resemblance of its active site structure to that of natural peroxidase enzymes. A-Cu demonstrated remarkable catalytic efficiency in POD-mimicking reactions and maintained in situ structural and functional stability during assay conditions. Capitalizing on this peroxidase-like activity, A-Cu was successfully applied as a nanozyme-based platform for the colorimetric detection of key biological targets—hydrogen peroxide (H_2O_2) and the neurotransmitter glutathione (GSH). The sensing system showed significant analytical performance with low limits of detection, measured at 6.8 μM for H_2O_2 and 2 μM for GSH, indicating strong potential for sensitive and reliable biosensing applications. Importantly, the biocompatibility of the A-Cu nanozyme was thoroughly evaluated to ensure its safe use in biological systems. Cytotoxicity studies using the MTT assay confirmed that A-Cu exhibits minimal toxicity toward living cells, suggesting favourable cellular compatibility. Furthermore, additional in vivo biocompatibility was assessed using the chicken egg chorioallantoic membrane (CAM) model, which further validated the material's non-toxic nature and its suitability for potential biomedical applications.

Overall, the findings presented in this chapter underscore the multifunctionality of the A-Cu bionanozyme, highlighting not only its catalytic versatility and sensitivity in biosensing but also its high level of biocompatibility. These attributes make A-Cu a highly promising candidate for future applications in areas such as diagnostic sensing, therapeutic monitoring, and environmentally friendly catalysis.

5.5 Experimental Section:

1) POD-mimicking catalytic assay, kinetics, and stability experiments

a) POD-mimicking catalytic assay of A-Cu: The POD activity of A-Cu was studied by using the colorimetric method. Hydrogen peroxide (H_2O_2) was used as a substrate and TMB was used as a colorimetric reagent. To perform this experiment, 1 mM of H_2O_2 (Stock solution of 50 mM in water) was added to PBS (1X) buffer of optimum pH-4, then 0.2 mM TMB (Stock solution of 21 mM in DMSO) and 0.2 mg/mL of A-Cu (Stock solution of 1 mg/mL in water) was added to the reaction mixture and total volume were made 2 mL. Then the sample was filled in a 3.5 mL quartz cuvette to perform the UV-visible spectra. In UV-vis spectra, an absorption band was observed at 652 nm which corresponds to ^{ox}TMB.[48]

b) Control studies: Control experiments were performed by mixing each component like H_2O_2 (1 mM), TMB (0.2 mM), A (0.1 mM), $CuCl_2$ (0.1 mM), and A-Cu (0.1 mM) to PBS buffer. Interestingly, there was no intense blue coloration or absorbance band observed in any other case except the combination of (H_2O_2+TMB+A-Cu).

c) pH Effect: A combination of A-Cu (0.2 mg/mL), TMB (0.2 mM), and H_2O_2 (1 mM) was made in PBS buffers in the range of pH from 3 to 9 at room temperature. The optimum POD-like activity we have is an acidic pH of 4.

d) Substrate-dependent kinetics: Next, substrate-dependent kinetics were performed by varying the concentration of H_2O_2 with a fixed optimum concentration of TMB, which is based on the first curve of saturated concentrations as shown in **(Figure 4b)** (0.2 mM) and A-Cu (0.2 mg/ml). To determine the initial reaction rate (V_0), different concentrations of DP (0, 0.02, 0.04, 0.06, 0.08, 0.1, 0.2, 0.3, 0.4, 0.5, 0.6, 0.7, 0.8, 0.9 and 1 mM) were reacted with 0.5 mM of AP, catalysed by 0.2 mg/mL of catalyst A-Cu. Then each sample corresponds to H_2O_2 and immediately records the kinetics by monitoring the band at 652 nm which corresponds to ^{ox}TMB. The obtained data were fitted into the Michaelis–Menten model to extract the kinetics parameters K_m and V_{max}.

e) Detection of H_2O_2 by using POD-mimicking catalytic activity of A-Cu: Concentration of H_2O_2 from (10, 20, 30, 40, 50, 70, 80, 90, 100, 110 μM) was added with fixed concentration of TMB (0.2 mM) and A-Cu (0.2 mg/mL) in PBS buffer (pH-4) as reaction medium and total volume was made 2 mL. After the addition of the A-Cu sample was incubated for 5 minutes and employed for UV-vis spectra. With raises in the concentration of H_2O_2, there is a continuous increment of the band at 652 nm observed in UV-vis spectra. Next, to calculate

the limit of detection (LOD), the standard linear curve was plotted between the concentration of H_2O_2 and the change in absorbance at 652 nm.

2) Colorimetric detection of antioxidant compound glutathione (GSH)

a) Variable concentrations of GSH (0, 10, 20, 30, 40, 50, 60, 70, 80, 100, 120, 140 μM) were added into the POD system which is a combination of A-Cu (0.2 mg/mL), TMB (0.2 mM) and H_2O_2 (1 mM) by maintaining same time interval of 2 minutes which is minimum time of saturation POD reaction progress at 25 ^{o}C. Next, after adding each concentration of GSH, UV spectra were recorded by using a 3.5 mL quartz cuvette. It was observed that on increasing GSH content the band corresponding to ^{ox}TMB decreased continuously. Next, a plot was constructed between absorbance at 652 nm vs [GSH] (μM). A linear standard curve was obtained in the concentration range of 0-80 μM. Next, LOD=2 μM was calculated to correspond to the minimum concentration range.

b) Interference studies were conducted by adding the concentration of 140 μM (stock solution: 1mM solvent water) for each analyte, as determined by the maximum concentration of GSH shown in **Figure 8**. These analytes were added to the peroxidase system as described in Section 6a. Following the addition of the interfering analytes, UV-visible spectra were recorded for each sample in a PBS buffer at pH 4.0, with measurements taken at room temperature after an incubation period of 2 minutes for each analyte.

3) Cytotoxicity and *in vivo* biocompatibility of A-Cu Bionanozyme:

a) Using the chorioallantoic membrane (CAM) experiment, evaluate biocompatibility of A-Cu Bionanozyme: In this work, the CAM assay was used to inspect the biocompatibility of A-Cu on the development of blood arteries in the chicken embryo. For this experiment, fertilized eggs were obtained from a hatchery located in Varanasi, Uttar Pradesh. After that, the eggs were incubated at 37 °C for four days. The egg's outer shell was slightly punctured on the fifth day to reveal the evolving blood vessels. The chick embryo was treated with A-Cu (0.1 mg/mL) for two minutes at room temperature, and then Whatman filter paper discs were placed over its blood vessels. For a maximum of six hours, the effects of A-Cu on blood vessel creation and development were seen using a Magnus MagZoom TZM6 Trinocular Stereo Zoom Microscope. Untreated eggs were used as a control. Additionally, blood artery integrity parameters like length, junctions, and size were measured using the applications Angiotool and ImageJ.[49]

b) Investigation of cell viability using the MTT assay: The outcome of A-Cu on the cell viability of the embryonic mouse fibroblast (NIH3T3) and Human Embryonic Kidney cell line was examined using the MTT assay. 96-well plates were seeded with 10,000/100 µL DMEM medium. Three different dosages of A-Cu (1 mg/mL, 0.5 mg/mL, and 0.1 mg/mL) were added as treatments after a 24-hour incubation period. Following the medium removal, 100 µL (0.5 mg/mL) solution of MTT was included, and the combination was left to incubate for four hours at 37 °C. The formazan crystal was dissolved by adding 100 µL of DMSO: MeOH (1:1) after discarding the MTT solutions. A multiple reader was employed to measure the absorbance of the combination at 570 nm following that, the formula below was utilized to ascertain the cell viability.

$$\% \text{ cell viability} = (\text{Absorbance}_S / \text{Absorbance}_C) \times 100$$

Absorbance S and Absorbance C denote the absorbance of the sample and control at 570 nm.

c) Measurement of cellular internalized ROS: In 24-well culture dishes, cancer cells (KBCHR8,5; 20,000 cells per well) were cultivated for 24 hours in the cell culture incubator, at 37 °C. Three types of cells were used to treat the cancer cell lines: untreated cells, cells with H_2O_2 (300 µM), and cells with varying concentrations of A-Cu. The concentrations of A-Cu used were 0.1 mg/mL, 0.5 mg/mL, and 1 mg/mL. After eight hours, each well received 10 µL of 2′,7′-Dichlorofluorescin Diacetate (DCFDA) (30 µM), which was then left for thirty to forty minutes. PBS was used to properly wash the incubated cells two or three times. Following that confocal images were taken; Zeiss 510 Meta confocal microscopy equipment was used to capture images at 20X**.** Also, 100 µL of Radioimmunoprecipitation assay (RIPA) buffer was added to the cells to lyse them, and they were maintained for 10 minutes at 4 °C. Centrifuging the scraped cells for 10 minutes at 4 °C at 14,000 rpm yielded cell lysates. The fluorescence of both treated and untreated cells was measured using a multimode reader with an excitation at λ_{ex} = 380 nm and an emission at λ_{em} = 460 nm.

d) Live Dead Assay

Cell viability was determined using a live/dead ™ Cell Imaging kit R37601. In accordance with the manufacturer's protocol, cells were washed with PBS twice and exposed to **Component A (Live Green)** cell-permeant calcein, AM which is hydrolyzed by intracellular esterases, and to, **Component B (Dead Red)** which binds to nucleic acids. The cleavage product of calcein AM, calcein, produces a green fluorescence when exposed to 488-nm light and can be used to identify live cells. Dead red produces a red fluorescence when exposed to

570-nm light, allowing the identification of dead cells. Culture dishes were dually stained and examined under a fluorescence microscope system (Zeiss 510 Meta confocal microscopy equipment) was used to capture images of live and dead bacteria at 63 X).

e) Statistical analysis: To ensure precision and credibility, the trials were carried out three times. The mean value and standard error were used to express the data from each experiment. A one-way ANOVA was performed using the Origin software to ascertain the statistical significance of the obtained data.

5.6 References

(1) Robinson, P. K. Enzymes: Principles and Biotechnological Applications. *Essays Biochem.* **2015**, *59*, 1–41. https://doi.org/10.1042/BSE0590001.

(2) Gajhede, M.; Schuller, D. J.; Henriksen, A.; Smith, A. T.; Poulos, T. L. Crystal Structure of Horseradish Peroxidase C at 2.15 Å Resolution. *Nat. Struct. Biol.* **1997**, *4* (12), 1032–1038. https://doi.org/10.1038/nsb1297-1032.

(3) Campomanes, P.; Rothlisberger, U.; Alfonso-Prieto, M.; Rovira, C. The Molecular Mechanism of the Catalase-like Activity in Horseradish Peroxidase. *J. Am. Chem. Soc.* **2015**, *137* (34), 11170–11178. https://doi.org/10.1021/jacs.5b06796.

(4) Guan, M.; Wang, M.; Qi, W.; Su, R.; He, Z. Biomineralization-Inspired Copper-Cystine Nanoleaves Capable of Laccase-like Catalysis for the Colorimetric Detection of Epinephrine. *Front. Chem. Sci. Eng.* **2021**, *15* (2), 310–318. https://doi.org/10.1007/s11705-020-1940-y.

(5) Makam, P.; Yamijala, S. S. R. K. C.; Bhadram, V. S.; Shimon, L. J. W.; Wong, B. M.; Gazit, E. Single Amino Acid Bionanozyme for Environmental Remediation. *Nat. Commun.* **2022**, *13* (1), 1505. https://doi.org/10.1038/s41467-022-28942-0.

(6) Wu, J.; Wang, X.; Wang, Q.; Lou, Z.; Li, S.; Zhu, Y.; Qin, L.; Wei, H. Nanomaterials with Enzyme-like Characteristics (Nanozymes): Next-Generation Artificial Enzymes (II). *Chem. Soc. Rev.* **2019**, *48* (4), 1004–1076. https://doi.org/10.1039/c8cs00457a.

(7) Chen, J.; Huang, L.; Wang, Q.; Wu, W.; Zhang, H.; Fang, Y.; Dong, S. Bio-Inspired Nanozyme: A Hydratase Mimic in a Zeolitic Imidazolate Framework. *Nanoscale* **2019**, *11* (13), 5960–5966. https://doi.org/10.1039/C9NR01093A.

(8) Gao, L.; Zhuang, J.; Nie, L.; Zhang, J.; Zhang, Y.; Gu, N.; Wang, T.; Feng, J.; Yang, D.; Perrett, S.; Yan, X. Intrinsic Peroxidase-like Activity of Ferromagnetic Nanoparticles. *Nat. Nanotechnol.* **2007**, *2* (9), 577–583. https://doi.org/10.1038/nnano.2007.260.

(9) Gao, L.; Fan, K.; Yan, X. Iron Oxide Nanozyme: A Multifunctional Enzyme Mimetic for Biomedical Applications. *Theranostics* **2017**, *7* (13), 3207–3227. https://doi.org/10.7150/thno.19738.

(10) Fang, M.; Zheng, R.; Wu, Y.; Yue, D.; Qian, X.; Zhao, Y.; Bian, Z. CuO Nanosheet as a Recyclable Fenton-like Catalyst Prepared from Simulated Cu(Ii) Waste Effluents by Alkaline H 2 O 2 Reaction. *Environ. Sci. Nano* **2019**, *6* (1), 105–114. https://doi.org/10.1039/c8en00930a.

(11) Lee, H.; Seong, J.; Lee, K. M.; Kim, H. H.; Choi, J.; Kim, J. H.; Lee, C. Chloride-Enhanced Oxidation of Organic Contaminants by Cu(II)-Catalyzed Fenton-like Reaction at Neutral PH. *J. Hazard. Mater.* **2018**, *344* (October 2017), 1174–1180. https://doi.org/10.1016/j.jhazmat.2017.10.020.

(12) Geng, X.; Xie, X.; Liang, Y.; Li, Z.; Yang, K.; Tao, J.; Zhang, H.; Wang, Z. Facile

Fabrication of a Novel Copper Nanozyme for Efficient Dye Degradation. *ACS Omega* **2021**, *6* (9), 6284–6291. https://doi.org/10.1021/acsomega.0c05925.

(13) Jiang, B.; Duan, D.; Gao, L.; Zhou, M.; Fan, K.; Tang, Y.; Xi, J.; Bi, Y.; Tong, Z.; Gao, G. F.; Xie, N.; Tang, A.; Nie, G.; Liang, M.; Yan, X. Standardized Assays for Determining the Catalytic Activity and Kinetics of Peroxidase-like Nanozymes. *Nat. Protoc.* **2018**, *13* (7), 1506–1520. https://doi.org/10.1038/s41596-018-0001-1.

(14) Wu, J.; Wang, X.; Wang, Q.; Lou, Z.; Li, S.; Zhu, Y.; Qin, L.; Wei, H. Nanomaterials with Enzyme-like Characteristics (Nanozymes): Next-Generation Artificial Enzymes (II). *Chem. Soc. Rev.* **2019**, *48* (4), 1004–1076. https://doi.org/10.1039/C8CS00457A.

(15) Tsuneda, T. Fenton Reaction Mechanism Generating No OH Radicals in Nafion Membrane Decomposition. *Sci. Rep.* **2020**, *10* (1), 1–13. https://doi.org/10.1038/s41598-020-74646-0.

(16) Zhang, X.; Huang, Y. Evaluation of the Antioxidant Activity of Phenols and Tannic Acid Determination with Mn 3 O 4 Nano-Octahedrons as an Oxidase Mimic. *Anal. Methods* **2015**, *7* (20), 8640–8646. https://doi.org/10.1039/C5AY01732G.

(17) Xu, B.; Li, S.; Zheng, L.; Liu, Y.; Han, A.; Zhang, J.; Huang, Z.; Xie, H.; Fan, K.; Gao, L.; Liu, H. A Bioinspired Five-Coordinated Single-Atom Iron Nanozyme for Tumor Catalytic Therapy. *Adv. Mater.* **2022**, *34* (15), 1–9. https://doi.org/10.1002/adma.202107088.

(18) Fan, K.; Wang, H.; Xi, J.; Liu, Q.; Meng, X.; Duan, D.; Gao, L.; Yan, X. Optimization of Fe3O4 Nanozyme Activity via Single Amino Acid Modification Mimicking an Enzyme Active Site. *Chem. Commun.* **2017**, *53* (2), 424–427. https://doi.org/10.1039/c6cc08542c.

(19) Tian, Z.; Li, J.; Zhang, Z.; Gao, W.; Zhou, X.; Qu, Y. Highly Sensitive and Robust Peroxidase-like Activity of Porous Nanorods of Ceria and Their Application for Breast Cancer Detection. *Biomaterials* **2015**, *59*, 116–124. https://doi.org/10.1016/j.biomaterials.2015.04.039.

(20) Cao, W.; Ju, P.; Wang, Z.; Zhang, Y.; Zhai, X.; Jiang, F.; Sun, C. Colorimetric Detection of H2O2 Based on the Enhanced Peroxidase Mimetic Activity of Nanoparticles Decorated Ce2(WO4)3 Nanosheets. *Spectrochim. Acta Part A Mol. Biomol. Spectrosc.* **2020**, *239*, 118499. https://doi.org/10.1016/j.saa.2020.118499.

(21) Yin, S.-J.; Chen, G.-Y.; Zhang, C.-Y.; Wang, J.-L.; Yang, F.-Q. Zeolitic Imidazolate Frameworks as Light-Responsive Oxidase-like Mimics for the Determination of Adenosine Triphosphate and Discrimination of Phenolic Pollutants. *Microchim. Acta* **2023**, *190* (1), 25. https://doi.org/10.1007/s00604-022-05602-0.

(22) Song, W.; Sun, P.; Zhou, J.; Han, X.; Dai, Q.; Chai, F. The Fabrication of CuBTC@PW 12 with Prominent Peroxidase-Mimicking Activity for Colorimetric Detection of H 2 O 2 and Ascorbic Acid via "on–off" Switch. *New J. Chem.* **2023**, *47* (33), 15721–15730. https://doi.org/10.1039/D3NJ02611F.

(23) Chen, C.; Wang, Y.; Zhang, D. Peroxidase-like Activity of Vanadium Tetrasulfide Submicrospheres and Its Application to the Colorimetric Detection of Hydrogen Peroxide and L-Cysteine. *Microchim. Acta* **2019**, *186* (12), 784. https://doi.org/10.1007/s00604-019-3942-3.

(24) Padamati, S. K.; Vedelaar, T. A.; Perona Martínez, F.; Nusantara, A. C.; Schirhagl, R. Insight into a Fenton-like Reaction Using Nanodiamond Based Relaxometry. *Nanomaterials* **2022**, *12* (14), 2422. https://doi.org/10.3390/nano12142422.

(25) Ding, Y.; Yang, B.; Liu, H.; Liu, Z.; Zhang, X.; Zheng, X.; Liu, Q. FePt-Au Ternary Metallic Nanoparticles with the Enhanced Peroxidase-like Activity for Ultrafast Colorimetric Detection of H2O2. *Sensors Actuators, B Chem.* **2018**, *259*, 775–783. https://doi.org/10.1016/j.snb.2017.12.115.

(26) Ding, Y.; Liu, H.; Gao, L.-N.; Fu, M.; Luo, X.; Zhang, X.; Liu, Q.; Zeng, R.-C. Fe-Doped Ag2S with Excellent Peroxidase-like Activity for Colorimetric Determination of H2O2. *J. Alloys Compd.* **2019**, *785*, 1189–1197. https://doi.org/10.1016/j.jallcom.2019.01.225.

(27) Yang, H.; Zha, J.; Zhang, P.; Xiong, Y.; Su, L.; Ye, F. Sphere-like CoS with Nanostructures as Peroxidase Mimics for Colorimetric Determination of H2O2 and Mercury Ions. *RSC Adv.* **2016**, *6* (71), 66963–66970. https://doi.org/10.1039/c6ra16619a.

(28) Wang, N.; Sun, J.; Chen, L.; Fan, H.; Ai, S. A Cu2(OH)3Cl-CeO2 Nanocomposite with Peroxidase-like Activity, and Its Application to the Determination of Hydrogen Peroxide, Glucose and Cholesterol. *Microchim. Acta* **2015**, *182* (9–10), 1733–1738. https://doi.org/10.1007/s00604-015-1506-8.

(29) Liu, Q.; Tang, P.; Xing, X.; Cheng, W.; Liu, S.; Lu, X.; Zhong, L. Colorimetry /SERS Dual-Sensor of H2O2 Constructed via TMB–Fe3O4@ AuNPs. *Talanta* **2022**, *240* (August 2021), 123118. https://doi.org/10.1016/j.talanta.2021.123118.

(30) Zhang, C.-Y.; Peng, L.-J.; Chen, G.-Y.; Zhang, H.; Yang, F.-Q. Investigation on the Peroxidase-like Activity of Vitamin B6 and Its Applications in Colorimetric Detection of Hydrogen Peroxide and Total Antioxidant Capacity Evaluation. *Molecules* **2022**, *27* (13), 4262. https://doi.org/10.3390/molecules27134262.

(31) Lee, G.; Kim, C.; Kim, D.; Hong, C.; Kim, T.; Lee, M.; Lee, K. Multibranched Au–Ag–Pt Nanoparticle as a Nanozyme for the Colorimetric Assay of Hydrogen Peroxide and Glucose. *ACS Omega* **2022**, *7* (45), 40973–40982. https://doi.org/10.1021/acsomega.2c04129.

(32) Li, P.; Lee, S. M.; Kim, H. Y.; Kim, S.; Park, S.; Park, K. S.; Park, H. G. Colorimetric Detection of Individual Biothiols by Tailor Made Reactions with Silver Nanoprisms. *Sci. Rep.* **2021**, *11* (1), 3937. https://doi.org/10.1038/s41598-021-83433-4.

(33) Liu, J.; Meng, L.; Fei, Z.; Dyson, P. J.; Jing, X.; Liu, X. MnO 2 Nanosheets as an Artificial Enzyme to Mimic Oxidase for Rapid and Sensitive Detection of Glutathione.

Biosens. Bioelectron. **2017**, *90* (September 2016), 69–74. https://doi.org/10.1016/j.bios.2016.11.046.

(34) Zhu, X.; Li, H.; Zhang, D.; Chen, W.; Fu, M.; Nie, S.; Gao, Y.; Liu, Q. Novel "On–Off" Colorimetric Sensor for Glutathione Based on Peroxidase Activity of Montmorillonite-Loaded TiO 2 Functionalized by Porphyrin Precisely Controlled by Visible Light. *ACS Sustain. Chem. Eng.* **2019**, *7* (21), 18105–18113. https://doi.org/10.1021/acssuschemeng.9b05146.

(35) Zou, H.; Yang, T.; Lan, J.; Huang, C. Use of the Peroxidase Mimetic Activity of Erythrocyte-like Cu 1.8 S Nanoparticles in the Colorimetric Determination of Glutathione. *Anal. Methods* **2017**, *9* (5), 841–846. https://doi.org/10.1039/C6AY03034C.

(36) Cheng, X.; Zhou, X.; Zheng, Z.; Kuang, Q. Construct Efficient Substrate Transport and Catalytic Sub-Nanochannels in Metal-Organic Framework-Based Nanozymes for Boosting Peroxidase-like Catalytic Activity. *Chem. Eng. J.* **2022**, *430* (P3), 133079. https://doi.org/10.1016/j.cej.2021.133079.

(37) Zhao, X.; Wu, K.; Lyu, H.; Zhang, X.; Liu, Z.; Fan, G.; Zhang, X.; Zhu, X.; Liu, Q. Porphyrin Functionalized Co(OH)2/GO Nanocomposites as an Excellent Peroxidase Mimic for Colorimetric Biosensing. *Analyst* **2019**, *144* (17), 5284–5291. https://doi.org/10.1039/c9an00945k.

(38) Ma, Y.; Zhang, Z.; Ren, C.; Liu, G.; Chen, X. A Novel Colorimetric Determination of Reduced Glutathione in A549 Cells Based on Fe3O4 Magnetic Nanoparticles as Peroxidase Mimetics. *Analyst* **2012**, *137* (2), 485–489. https://doi.org/10.1039/c1an15718c.

(39) Xu, H.; Wang, Y.; Huang, X.; Li, Y.; Zhang, H.; Zhong, X. Hg 2+ -Mediated Aggregation of Gold Nanoparticles for Colorimetric Screening of Biothiols. *Analyst* **2012**, *137* (4), 924–931. https://doi.org/10.1039/C2AN15926K.

(40) Li, L.; Wang, Q.; Chen, Z. Colorimetric Detection of Glutathione Based on Its Inhibitory Effect on the Peroxidase-Mimicking Properties of WS2 Nanosheets. *Microchim. Acta* **2019**, *186* (4), 257. https://doi.org/10.1007/s00604-019-3365-1.

(41) Liu, X.; Wang, Q.; Zhang, Y.; Zhang, L.; Su, Y.; Lv, Y. Colorimetric Detection of Glutathione in Human Blood Serum Based on the Reduction of Oxidized TMB. *New J. Chem.* **2013**, *37* (7), 2174–2178. https://doi.org/10.1039/c3nj40897c.

(42) Ortiz-Gómez, I.; Rivadeneyra, A.; Salmerón, J. F.; Orbe-Payá, I. de; Morales, D. P.; Capitán-Vallvey, L. F.; Salinas-Castillo, A. Near-Field Communication Tag for Colorimetric Glutathione Determination with a Paper-Based Microfluidic Device. *Biosensors* **2023**, *13* (2), 267. https://doi.org/10.3390/bios13020267.

(43) Banerjee, D.; Vishwakarma, S.; Nayak, M.; Upadhyay, A.; Pradhan, L.; Makam, P.; Mukherjee, S. Fabrication of Zinc-Tryptophan Nanoassemblies for Antibacterial and Wound Healing Applications. *ACS Appl. Nano Mater.* **2025**, *8* (8), 4263–4278.

https://doi.org/10.1021/acsanm.5c00657.

(44) Chowdhury, S. R.; Mukherjee, S.; Das, S.; Patra, C. R.; Iyer, P. K. Multifunctional (3-in-1) Cancer Theranostics Applications of Hydroxyquinoline-Appended Polyfluorene Nanoparticles. *Chem. Sci.* **2017**, *8* (11), 7566–7575. https://doi.org/10.1039/C7SC03321D.

(45) Moreno-Jiménez, I.; Hulsart-Billstrom, G.; Lanham, S. A.; Janeczek, A. A.; Kontouli, N.; Kanczler, J. M.; Evans, N. D.; Oreffo, R. O. C. The Chorioallantoic Membrane (CAM) Assay for the Study of Human Bone Regeneration: A Refinement Animal Model for Tissue Engineering. *Sci. Rep.* **2016**, *6* (1), 32168. https://doi.org/10.1038/srep32168.

(46) Gambini, J.; Stromsnes, K. Oxidative Stress and Inflammation: From Mechanisms to Therapeutic Approaches. *Biomedicines* **2022**, *10* (4), 753. https://doi.org/10.3390/biomedicines10040753.

(47) Sun, T.; Xiao, S.; Wang, M.; Xie, Q.; Zhang, L.; Zhou, C.; Gong, M.; Zhang, D. Reactive Oxygen Species Scavenging Nanozymes: Emerging Therapeutics for Acute Liver Injury Alleviation. *Int. J. Nanomedicine* **2023**, *18* (December), 7901–7922. https://doi.org/10.2147/IJN.S435544.

(48) Huang, S.; Chen, G.; Ye, N.; Kou, X.; Zhang, R.; Shen, J.; Ouyang, G. Iron-Mineralization-Induced Mesoporous Metal-Organic Frameworks Enable High-Efficiency Synergistic Catalysis of Natural/Nanomimic Enzymes. *ACS Appl. Mater. Interfaces* **2020**, *12* (51), 57343–57351. https://doi.org/10.1021/acsami.0c16689.

(49) Pradhan, L.; Sah, P.; Nayak, M.; Upadhyay, A.; Pragya, P.; Tripathi, S.; Singh, G.; Mounika, B.; Paik, P.; Mukherjee, S. Biosynthesized Silver Nanoparticles Prevent Bacterial Infection in Chicken Egg Model and Mitigate Biofilm Formation on Medical Catheters. *JBIC J. Biol. Inorg. Chem.* **2024**, *29* (3), 353–373. https://doi.org/10.1007/s00775-024-02050-4.